Journal of Solid Mechanics Vol. 8, No. 4 (2016) pp. 788-805

Thermo-Mechanical Vibration Analysis of FG Circular and Annular Nanoplate Based on the Visco-Pasternak Foundation

M. Goodarzi [1, *], M. Mohammadi [1], M. Khooran [2], F. Saadi [1]

[1] *Department of Engineering, College of Mechanical Engineering, Ahvaz Branch, Islamic Azad University, Ahvaz, Iran*
[2] *Department of Mechanical Engineering, Shahid Chamran University of Ahvaz, Iran*

Received 23 July 2016; accepted 28 September 2016

ABSTRACT

In this study, the vibration behavior of functional graded (FG) circular and annular nanoplate embedded in a Visco-Pasternak foundation and coupled with temperature change is studied. The effect of in-plane pre-load and temperature change are investigated on the vibration frequencies of FG circular and annular nanoplate. To obtain the vibration frequencies of the FG circular and annular nanoplate, two different size dependent theories are utilized. The material properties of the FGM nanoplates are assumed to vary in the thickness direction and are estimated through the Mori–Tanaka homogenization technique. The FG circular and annular nanoplate is coupled by an enclosing viscoelastic medium which is simulated as a Visco-Pasternak foundation. By using the modified strain gradient theory (MSGT) and the modified couple stress theory (MCST), the governing equation is derived for FG circular and annular nanoplate. The differential quadrature method (DQM) and the Galerkin method (GM) are utilized to solve the governing equation to obtain the frequency vibration of FG circular and annular nanoplate. The results are subsequently compared with valid result reported in the literature. The effects of the size dependent, the in-plane pre-load, the temperature change, the power index parameter, the elastic medium and the boundary conditions on the natural frequencies are investigated. The results show that the size dependent parameter has an increasing effect on the vibration response of circular and annular nanoplate. The temperature change also play an important role in the mechanical behavior of the FG circular and annular nanoplate. The present analysis results can be used for the design of the next generation of nanodevices that make use of the thermal vibration properties of the nanoplate.

© 2016 IAU, Arak Branch.All rights reserved.

Keywords : Circular and annular nanoplate; Functional graded nanoplate; Modified strain gradient theory; Modified couple stress theory.

1 INTRODUCTION

THE concept of FGMs was first considered in Japan in 1984 during a space plane project, thereafter FGMs, due to their specific changing in their material properties, were developed for a wide range of applications, such as automotive industries, space vehicles, biomedical materials, reactor vessels, military applications, semiconductor industry and general structural elements in high thermal environments [1-3], and wide research efforts in many

*Corresponding author. Tel.: +98 9160085080.
E-mail address: m.goodarzi.iau@gmail.com (M.Goodarzi).

© 2016 IAU, Arak Branch. All rights reserved.

engineering fields during the recent years. Recently, FGMs are widely used in micro and nano-electromechanical systems (MEMS and NEMS) [4–8] and also atomic force microscopes (AFMs) [9]. So, analysis of the static and dynamic behavior of FGM structures under different actuation is very important.

Continuum modeling of the nanostructure has also increasing deal of attention of many researchers due to experiments in nanoscale are difficult [10] and molecular dynamic simulations are highly computationally expensive. Because of difficulties encountered in the experimental methods to predict the responses of nanostructures under different loading conditions as the size of physical systems is scaled down into the nanoscale, theoretical analyses have been more noteworthy. There are various size-dependent continuum theories such as couple stress theory [11], strain gradient elasticity theory [12], modified couple stress theory [13] and nonlocal elasticity theory [14-29]. Among these theories, modified strain gradient theory is one of the most applied theoretical approaches for the investigation of nano-mechanics due to their computational efficiency and the capability to produce accurate results, which are comparable to the atomistic model ones.

The pull-instability of hydrostaticaly and electrostatically actuated circular microplate is analyzed by Mohammadi et al. [12]. Wang et al. [30] presented Timoshenko nano-beams formulations based on the modified strain gradient theory. Ansari et al. [31,32] investigated the linear and nonlinear vibration characteristics of FGM microbeams based on the strain gradient and Timoshenko beam theories. They found that the value of material property gradient index plays a more important role in the vibrational response of the FGM microbeams with lower slenderness ratios. Recently, Sahmani and Ansari [33] studied the free vibration response of functionally graded higher-order shear deformable microplates based on strain gradient elasticity theory. The nonlinear forced vibrations of a microbeam employing strain gradient elasticity theory were investigated by Ghayesh et al. [34].

Mohammadi et al. [35] investigated the buckling of rectangular nanoplate under shear in-plane load and in thermal environment. They showed that the critical shear buckling load of rectangular nanoplate is strongly dependent on the small scale coefficient. Civalek and Akgoz [36] analyzed the vibration behavior of micro-scaled sector shaped graphene surrounded by an elastic matrix. Murmu and Pradhan [37] employed the nonlocal elasticity theory for the vibration analysis of rectangular single layered graphene sheets (SLGSs) embedded in an elastic medium. They have used both Winkler-type and Pasternak-type models for simulate the interaction of the graphene sheets with a surrounding elastic medium. They reported that the natural frequencies of SLGSs are strongly dependent on the small scale coefficients. Pradhan and Phadikar [38] investigated the vibration of embedded multilayered graphene sheets (MLGS) based on nonlocal continuum models. In thier paper, they have shown that nonlocal effect is quite significant and needs to be included in the continuum model of graphene sheet. Yi-Ze Wang et al. [39] studied the vibration of double-layered nanoplate. In their research, it is concluded thermal effect and nanoplate with isotropic mechanical properties. It has been reported that graphene sheets have orthotropic properties [40]. Aksencer and Aydogdu [41] proposed levy type solution for vibration and buckling of nanoplate. In that paper, they considered rectangular nanoplate with isotropic property and without effect of elastic medium. Malekzadeh et al. [42] used the differential quadrature method (DQM) to study the thermal buckling of a quadrilateral nanoplates embedded in an elastic medium. Thermal vibration analysis of orthotropic nanoplates based on nonlocal continuum mechanics were studied by Satish et al. [43] who considerate two variable refined plate theory for thermal vibration of orthotropic nanoplate. In general, SLGSs are embedded in an elastic medium but they did not consider effect of elastic medium in that paper. On the other hand, they represented vibration frequency of rectangular nanoplate only for simply supported boundary conditions and they did not represent vibration frequency for other boundary conditions. Prasanna Kumar et al. [44] represented thermal vibration analysis of monolayer graphene sheet embedded in an elastic medium via nonlocal continuum theory. In their paper, they considered simply support boundary condition and they did not study other boundary condition. They investigated graphene sheet with isotropic property. Farajpour et al. [45] studied axisymmetric buckling of the circular graphene sheets with the nonlocal continuum plate model. In that paper, the buckling behavior of circular nanoplates under uniform radial compression is studied. Explicit expressions for the buckling loads are obtained for clamped and simply supported boundary conditions. It is shown that nonlocal effects play an important role in the buckling of circular nanoplates. In that paper, their results compared with the results obtained by molecular dynamic and it is observed that results predicted by nonlocal theory are in exactly match with MD results. Thus the reliability of nonlocal theory and presented solution is demonstrated. Mohammadi et al [46] employed the nonlocal plate theory to analyze vibration of circular and annular graphene sheet. They founded that scale effect is less prominent in lower vibration mode numbers and is highly prominent in higher mode numbers.

It is cleared that the natural frequency is easily affected by the applied in-plane pre-load and temperature change. As a result, the effect of in-plane pre-load on the property of transverse vibration of functional graded circular and annular nanoplate is one of the practical interesting subjects. Researches that investigated on the FG circular and annular nanoplate are very limited in number with respect to the case of rectangular nanoplate. To the best

© 2016 IAU, Arak Branch

knowledge of the authors, it is the first time that the modified couple stress theory has been successfully applied to investigate the vibration frequency of the FG circular and annular nanoplate embedded in a Visco-Pasternak elastic medium under thermal environment. The influence of the surrounding elastic medium on the frequency vibration of the FG circular and annular nanoplate is investigated. In the present paper, the effect of the in-plane pre-load and temperature change on the vibration frequency of FG circular and annular nanoplate is investigated. The governing equation of motion is derived using the modified couple stress theory. The DQM is utilized to solve the governing equations of FG circular and annular nanoplate with simply supported, clamped boundary conditions and mix of them. From the results, some new and absorbing phenomena can be observed. The present results would be useful to suitably design nano electro-mechanical system and micro electro-mechanical systems (NEMS/MEMS) devices using FG circular and annular nanoplate.

2 DIFFERENTIAL EQUATIONS FOR NANOPLATES

A mono-layered circular and annular nanoplate embedded in a Visco-Pasternak foundation is shown in Fig. 1, in which geometrical parameters of outer radius *a*, inner radius *b* and thickness *h* is also indicated. The FGM profile across the thickness direction of the plate, made of ceramic and metal constituent materials, may be assumed to follow a function form as P-FGM plates as:

$$\begin{Bmatrix} E(z) \\ \alpha(z) \\ \upsilon(z) \end{Bmatrix} = \begin{Bmatrix} E_m + (E_c - E_m) \\ \alpha_m + (\alpha_c - \alpha_m) \\ \upsilon_m + (\upsilon_c - \upsilon_m) \end{Bmatrix} \left(\frac{2z+h}{2h} \right)^k \qquad -\frac{h}{2} \le z \le \frac{h}{2} \tag{1}$$

where, the $E(z)$, $\alpha(z)$ and $\upsilon(z)$ are the Young's module, the thermal expansion and the Poisson's ratio, respectively. Here, the Kirchhoff plate theory is considered to study the mechanical behavior of FG annular and circular nanoplate in the thermal environment, because it is adequate in providing accurate bending results for the thin plate due to small thickness in comparison with radius. On the basis of the Kirchhoff plate theory, the displacement field can be expressed as:

$$u = -z\frac{\partial w(r,t)}{\partial r}, \quad \text{v=0, w=w(r,t)} \tag{2}$$

where w(r,t) is the displacement of the middle surface of the nanoplate at the point $(r,\theta,0)$. Due to lacking material length scales, the conventional continuum mechanics has not the capability to predict the size-dependent response of the nanostructures. So, the MSGT is used to interpret the size effect into the vibration analysis of a FG circular nanoplate. In comparison with the MCST, the MSGT contains two additional gradient tensors of the dilatation and the deviatoric stretch in addition to the symmetric rotation gradient tensor. Three independent material length scale parameters and two classical material constants for isotropic linear elastic materials are utilized to specify these tensors. For a continuum constructed by a linear elastic material occupying region Ω with infinitesimal deformations, the stored strain energy U_m can be defined as:

$$U_m = \frac{1}{2}\int_{\Omega} \left(\sigma_{ij}\varepsilon_{ij} + p_i\gamma_i + \tau_{ijk}^{(1)}\eta_{ijk}^{(1)} + m_{ij}^{(1)}x_{ij}^{(1)} \right) dv \tag{3}$$

In which the components of the strain tensor ε_{ij}, the dilatation gradient tensor γ_i, the deviatoric stretch gradient tensor $\eta_{ijk}^{(1)}$, and the symmetric rotation gradient tensor $x_{ij}^{(1)}$ are given as: [47]

© 2016 IAU, Arak Branch

$$x_{r\theta}^{(s)}=\frac{1}{2}(-\frac{\partial^2 w}{\partial r^2}+\frac{1}{r}\frac{\partial w}{\partial r}),\ \ \gamma_r=-z(\frac{\partial^3 w}{\partial r^3}+\frac{1}{r}\frac{\partial^2 w}{\partial r^2}-\frac{1}{r^2}\frac{\partial w}{\partial r}),\ \ \gamma_z=-(\frac{\partial^2 w}{\partial r^2}+\frac{1}{r}\frac{\partial w}{\partial r})$$
$$\eta_{rrr}^{(1)}=\frac{z}{5}(\frac{1}{r}\frac{\partial^2 w}{\partial r^2}-\frac{1}{r^2}\frac{\partial w}{\partial r}-2\frac{\partial^3 w}{\partial r^3}),\quad \eta_{r\theta\theta}^{(1)}=\eta_{\theta\theta r}^{(1)}=\eta_{\theta r\theta}^{(1)}=\frac{z}{15}(3\frac{\partial^3 w}{\partial r^3}+\frac{4}{r^2}\frac{\partial w}{\partial r}-\frac{4}{r}\frac{\partial^2 w}{\partial r^2})$$
$$\eta_{rrz}^{(1)}=\eta_{rzr}^{(1)}=\eta_{zrr}^{(1)}=\frac{1}{15}(\frac{1}{r}\frac{\partial w}{\partial r}-4\frac{\partial^2 w}{\partial r^2}),\ \ \eta_{z\theta\theta}^{(1)}=\eta_{\theta\theta z}^{(1)}=\eta_{\theta z\theta}^{(1)}=\frac{1}{15}(\frac{\partial^2 w}{\partial r^2}-\frac{4}{r}\frac{\partial w}{\partial r})$$
$$\eta_{rzz}^{(1)}=\eta_{zzr}^{(1)}=\eta_{zrz}^{(1)}=\frac{z}{15}(3\frac{\partial^3 w}{\partial r^3}-\frac{1}{r^2}\frac{\partial w}{\partial r}+\frac{1}{r}\frac{\partial^2 w}{\partial r^2}),\ \ \eta_{zzz}^{(1)}=\frac{1}{5}(\frac{\partial^2 w}{\partial r^2}+\frac{1}{r}\frac{\partial w}{\partial r}) \tag{4}$$

Based on the components of the kinematic parameters, which are effective on the strain energy density of the structure, the constitutive equation for a linear isotropic elastic material can be expressed by [47] as:

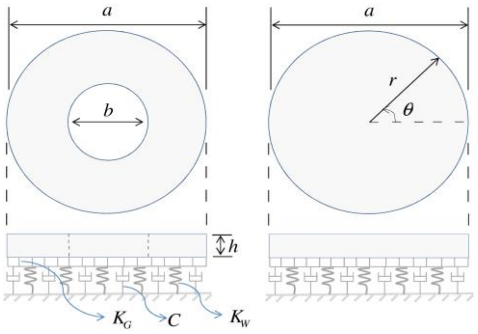

Fig.1
FG circular and annular nanoplate embedded on a Visco-Pasternak foundation.

$$m_{r\theta}^{(s)}=\mu(z)l_2^2(-\frac{\partial^2 w}{\partial r^2}+\frac{1}{r}\frac{\partial w}{\partial r}),\ \ p_r=-2z\mu(z)l_0^2(\frac{\partial^3 w}{\partial r^3}+\frac{1}{r}\frac{\partial^2 w}{\partial r^2}-\frac{1}{r^2}\frac{\partial w}{\partial r}),$$
$$p_z=-2\mu(z)l_0^2(\frac{\partial^2 w}{\partial r^2}+\frac{1}{r}\frac{\partial w}{\partial r})\tau_{rrr}^{(1)}=\frac{2z\mu(z)l_1^2}{5}(\frac{1}{r}\frac{\partial^2 w}{\partial r^2}-\frac{1}{r^2}\frac{\partial w}{\partial r}-2\frac{\partial^3 w}{\partial r^3}),$$
$$\tau_{rrz}^{(1)}=\tau_{rzr}^{(1)}=\tau_{zrr}^{(1)}=\frac{2\mu(z)l_1^2}{15}(\frac{1}{r}\frac{\partial w}{\partial r}-4\frac{\partial^2 w}{\partial r^2})$$
$$\tau_{r\theta\theta}^{(1)}=\tau_{\theta\theta r}^{(1)}=\tau_{\theta r\theta}^{(1)}=\frac{2z\mu(z)l_1^2}{15}(3\frac{\partial^3 w}{\partial r^3}+\frac{4}{r^2}\frac{\partial w}{\partial r}-\frac{4}{r}\frac{\partial^2 w}{\partial r^2}),\ \ \tau_{zzz}^{(1)}=\frac{2\mu(z)l_1^2}{5}(\frac{\partial^2 w}{\partial r^2}+\frac{1}{r}\frac{\partial w}{\partial r})$$
$$\tau_{z\theta\theta}^{(1)}=\tau_{\theta\theta z}^{(1)}=\tau_{\theta z\theta}^{(1)}=\frac{2\mu(z)l_1^2}{15}(\frac{\partial^2 w}{\partial r^2}-\frac{4}{r}\frac{\partial w}{\partial r})$$
$$\tau_{rzz}^{(1)}=\tau_{zzr}^{(1)}=\tau_{zrz}^{(1)}=\frac{2z\mu(z)l_1^2}{15}(3\frac{\partial^3 w}{\partial r^3}-\frac{1}{r^2}\frac{\partial w}{\partial r}+\frac{1}{r}\frac{\partial^2 w}{\partial r^2}),\ \ \varepsilon_{rr}=-z\frac{\partial^2 w}{\partial r^2},\ \ \varepsilon_{\theta\theta}=-\frac{z}{r}\frac{\partial w}{\partial r}$$
$$\sigma_{rr}=\frac{E(z)}{(1-\upsilon(z)^2)}\left(-z\left(\frac{\partial^2 w}{\partial r^2}+\frac{\upsilon(z)}{r}\frac{\partial w}{\partial r}\right)-\alpha(z)(1+\upsilon(z))T\right)$$
$$\sigma_{\theta\theta}=\frac{E(z)}{(1-\upsilon(z)^2)}\left(-z\left(\frac{1}{r}\frac{\partial w}{\partial r}+\upsilon(z)\frac{\partial^2 w}{\partial r^2}\right)-\alpha(z)(1+\upsilon(z))T\right) \tag{5}$$

The parameters λ and μ appeared in the constitutive equation of the classical stress σ, denote the Lame constants, respectively which are given as: [48]

$$\lambda(z)=\frac{\upsilon(z)E(z)}{(1-\upsilon(z)^2)},\quad \mu(z)=\frac{E(z)}{2(1+\upsilon(z))} \tag{6}$$

© 2016 IAU, Arak Branch

The corresponding components of the classical and nonclassical stresses can be evaluated by substituting the components of the strain tensor, the dilatation gradient tensor, the deviatoric stretch gradient tensor, and the symmetric rotation gradient tensor in Eq. (5). So, the strain energy Π_s based on Eq. (3) and kinetic energy of microplate Π_T can be written as:

$$\Pi_s = \frac{1}{2}\int_A \left(\begin{array}{l} -M_r w_{,rr} - M_\theta \frac{1}{r}\frac{\partial w}{\partial r} + Y_{r\theta}(\frac{1}{r}\frac{\partial w}{\partial r} - \frac{\partial^2 w}{\partial r^2}) - M_r^p(\frac{\partial^3 w}{\partial r^3} - \frac{1}{r^2}\frac{\partial w}{\partial r} + \frac{1}{r}\frac{\partial^2 w}{\partial r^2}) \\ -P_z(\frac{\partial^2 w}{\partial r^2} + \frac{1}{r}\frac{\partial w}{\partial r}) - T_{rrz}^\tau \frac{\partial^2 w}{\partial r^2} - M_{rrr}^\tau \frac{\partial^3 w}{\partial r^3} + M_{\theta\theta r}^\tau(\frac{1}{r^2}\frac{\partial w}{\partial r} - \frac{1}{r}\frac{\partial^2 w}{\partial r^2}) - \frac{T_{\theta\theta z}^\tau}{r}\frac{\partial w}{\partial r} \end{array} \right) dA$$

$$\Pi_T = \frac{1}{2}\int_A \left(I_1\left(\frac{\partial w}{\partial t}\right)^2 + I_2\left(\frac{\partial^2 w}{\partial r \partial t}\right)^2 \right) dA \tag{7}$$

where A denotes the area occupied by the mid-plane of the circular FG nanoplate. Moreover, I_1 and I_2 are represented as the following form:

$$I_2 = \int_{-h/2}^{h/2} \rho(z)dz, \quad I_1 = \int_{-h/2}^{h/2} \rho(z)z^2 dz \tag{8}$$

In Eq. (7), bending moments, couple moments, other higher-order resultants force and higher-order moments caused by higher-order stresses effective on the section are expressed as follows:

$$\begin{aligned}
M_{rr} &= \int_{-h/2}^{h/2} \frac{E(z)z}{(1-\upsilon^2)}\left(-z\left(\frac{\partial^2 w}{\partial r^2} + \frac{\upsilon}{r}\frac{\partial w}{\partial r}\right) - \alpha(z)(1+\upsilon)T\right)dz, \\
M_{\theta\theta} &= \int_{-h/2}^{h/2} \frac{E(z)z}{(1-\upsilon^2)}\left(-z\left(\frac{1}{r}\frac{\partial w}{\partial r} + \upsilon\frac{\partial^2 w}{\partial r^2}\right) - \alpha(z)(1+\upsilon)T\right)dz, \\
N_{rr} &= \int_{-h/2}^{h/2} \frac{E(z)}{(1-\upsilon^2)}\left(-z\left(\frac{\partial^2 w}{\partial r^2} + \frac{\upsilon}{r}\frac{\partial w}{\partial r}\right) - \alpha(z)(1+\upsilon)T\right)dz, \\
N_{\theta\theta} &= \int_{-h/2}^{h/2} \frac{E(z)}{(1-\upsilon^2)}\left(-z\left(\frac{1}{r}\frac{\partial w}{\partial r} + \upsilon\frac{\partial^2 w}{\partial r^2}\right) - \alpha(z)(1+\upsilon)T\right)dz, \\
Y_{r\theta} &= \int_{-h/2}^{h/2} \mu(z)l_2^2(-\frac{\partial^2 w}{\partial r^2} + \frac{1}{r}\frac{\partial w}{\partial r})dz, \qquad \mathrm{P}_z = -\int_{-h/2}^{h/2} 2\mu(z)l_0^2(\frac{\partial^2 w}{\partial r^2} + \frac{1}{r}\frac{\partial w}{\partial r})dz \\
M_r^p &= -\int_{-h/2}^{h/2} 2z\mu(z)l_0^2(\frac{\partial^2 w}{\partial r^2} + \frac{1}{r}\frac{\partial w}{\partial r})dz, \quad \mathrm{T}_{rrz}^\tau = \int_{-h/2}^{h/2} \frac{2\mu(z)l_1^2}{15}(\frac{1}{r}\frac{\partial w}{\partial r} - 4\frac{\partial^2 w}{\partial r^2})dz \\
\mathrm{T}_{\theta\theta z}^\tau &= \int_{-h/2}^{h/2} \frac{2\mu(z)l_1^2}{15}(\frac{\partial^2 w}{\partial r^2} - \frac{4}{r}\frac{\partial w}{\partial r})dz, \quad \mathrm{M}_{rrr}^\tau = \int_{-h/2}^{h/2} \frac{2z^2\mu(z)l_1^2}{5}(\frac{1}{r}\frac{\partial^2 w}{\partial r^2} - \frac{1}{r^2}\frac{\partial w}{\partial r} - 2\frac{\partial^3 w}{\partial r^3})dz \\
\mathrm{M}_{\theta\theta r}^\tau &= \int_{-h/2}^{h/2} \frac{2z^2\mu(z)l_1^2}{15}(3\frac{\partial^3 w}{\partial r^3} + \frac{4}{r^2}\frac{\partial w}{\partial r} - \frac{4}{r}\frac{\partial^2 w}{\partial r^2})dz
\end{aligned} \tag{9}$$

The value of the work done by the external forces applied on the plate can be expressed as:

$$W_{ext} = \int_A \left(qw(r,t) + fw(r,t)\right)dA \tag{10}$$

Here q and f are the distributed external force and the reaction force of elastic foundation, respectively. The reaction force of elastic foundation are expressed as:

© 2016 IAU, Arak Branch

$$f=\begin{cases} K_w w(r,t) & \text{The winkler foundation} \\ K_w w(r,t)-K_G\nabla^2 w(r,t) & \text{The Pasternak foundation} \\ K_w w(r,t)-K_G\nabla^2 w(r,t)+C_d\dfrac{\partial w(r,t)}{\partial t} & \text{The Visco-Pasternak foundation} \end{cases} \tag{11}$$

By using Hamilton's principle $\int_{t_1}^{t_2}(\Pi_s-\Pi_T-W_{ext})dt=0$ and taking the variation of w, integrating by parts and setting the coefficients of δw equal to zero leads to the following governing equation:

$$\begin{aligned} &M_{r,rr}+\frac{2M_{r,r}-M_{\theta,r}}{r}+\frac{3}{r}Y_{r\theta,r}+Y_{r\theta,rr}-\frac{2}{r}M^P_{r,rr}-M^P_{r,rrr}-\frac{M^P_r}{r^3}+\frac{M^P_{r,r}}{r^2}+\frac{P_{z,r}}{r}+P_{z,rr}+T_{rrz,rr} \\ &+\frac{2T_{rrz,r}}{r}-\frac{T_{\theta\theta z,r}}{r}-\frac{3M^\tau_{rrr,rr}}{r}-M^\tau_{rrr,rrr}-\frac{M^\tau_{\theta\theta r}}{r^3}+\frac{M^\tau_{\theta\theta r,r}}{r^2}+\frac{M^\tau_{\theta\theta r,rr}}{r}+f+q=I_1\frac{\partial^2 w}{\partial t^2}-I_2\frac{\partial^4 w}{\partial r^2\partial t^2} \end{aligned} \tag{12}$$

Also, the boundary conditions are obtained as the following form:

$$\begin{aligned} &\delta w=0 \quad \text{or} \quad -\mathrm{M}_r-rM_{r,r}+M_\theta-2Y_{r\theta}-rY_{r\theta,r}+M^p_{r,r}+rM^p_{r,rr}-\frac{M^p_r}{r}-rP_{z,r}-T^\tau_{rrz}-rT^\tau_{rrz,r} \\ &+T^\tau_{\theta\theta z}+2M^\tau_{rrr,r}+rM^\tau_{rrr,rr}-M^\tau_{\theta\theta r}-M^\tau_{\theta\theta r,r}=0 \\ &\frac{\partial\delta w}{\partial r}=0 \quad \text{or} \quad \mathrm{rM}_r+rY_{r\theta}-rM^p_{r,r}+rP_z+rT^\tau_{rrz}-M^\tau_{rrr}-rM^\tau_{rrr,r}+M^\tau_{\theta\theta r}=0 \\ &\frac{\partial^2\delta w}{\partial r^2}=0 \quad \text{or} \quad \mathrm{r}M^p_r+rM^\tau_{rrr}=0 \end{aligned} \tag{13}$$

By inserting the Eq. (8), the Eq. (9) and the Eq. (11) into the Eq. (12), the governing equation is obtained as the following form

$$\begin{aligned} &\left\{2l_0^2+\frac{4l_1^2}{5}\right\}A'\frac{\partial^6 w}{\partial r^6}+\left\{\frac{6l_0^2}{r}+\frac{12l_1^2}{5r}\right\}A'\frac{\partial^5 w}{\partial r^5}-\left\{C'+l_2^2B'+2l_0^2B'+\frac{2l_1^2}{15r^2}A'+\frac{8l_1^2}{15}B'\right\}\frac{\partial^4 w}{\partial r^4} \\ &-\left\{\frac{2}{r}C'+\frac{2l_2^2}{r}B'+\frac{4l_0^2}{r}B'+\frac{12l_0^2}{r^3}A'-\frac{16l_1^2}{15r}B'+\frac{4l_1^2}{15r^3}A'\right\}\frac{\partial^3 w}{\partial r^3} \\ &+\left\{\frac{1}{r^2}C'+\frac{l_2^2}{r^2}B'-\frac{18l_0^2}{r^4}A'+\frac{2l_0^2}{r^2}B'+\frac{8l_1^2}{15r^2}B'+N_0+N^*+K_G\right\}\frac{\partial^2 w}{\partial r^2} \\ &+\left\{-\frac{1}{r^3}C'-\frac{l_2^2}{r^3}B'+\frac{18l_0^2}{r^5}A'-\frac{2l_0^2}{r^3}B'-\frac{8l_1^2}{15r^3}B'+\frac{12l_1^2}{15r^4}A'+\frac{N_0}{r}+\frac{N^*}{r}+\frac{K_G}{r}\right\}\frac{\partial w}{\partial r} \\ &-K_w w-C_d\frac{\partial w}{\partial t}=I_1\frac{\partial^2 w}{\partial t^2}-I_2\frac{\partial^4 w}{\partial t^2\partial r^2} \end{aligned} \tag{14}$$

where the A', B' and C' are represented as the following:

© 2016 IAU, Arak Branch

$$
\begin{aligned}
&A' = \int_{-h/2}^{h/2} \mu_m z^2 + (\mu_c - \mu_m) z^2 \left(\frac{2z+h}{2h}\right)^k dz,\ \ B' = \int_{-h/2}^{h/2} \mu_m + (\mu_c - \mu_m)\left(\frac{2z+h}{2h}\right)^k dz,\\
&C' = \int_{-h/2}^{h/2} \left(E_m z^2 + (E_c - E_m) z^2 \left(\frac{2z+h}{2h}\right)^k\right) \Bigg/ \left(1 - \left(\upsilon_m + (\upsilon_c - \upsilon_m)\left(\frac{2z+h}{2h}\right)^k\right)^2\right) dz\\
&D' = \int_{-h/2}^{h/2} \rho_m + (\rho_c - \rho_m)\left(\frac{2z+h}{2h}\right)^k dz,\ \ E' = \int_{-h/2}^{h/2} \rho_m z^2 + (\rho_c - \rho_m) z^2 \left(\frac{2z+h}{2h}\right)^k dz,\\
&N^* = \int_{-h/2}^{h/2} \frac{\left(E_m + (E_c - E_m)\left(\frac{2z+h}{2h}\right)^k\right)}{\left(1 - \left(\upsilon_m + (\upsilon_c - \upsilon_m)\left(\frac{2z+h}{2h}\right)^k\right)\right)} \left(\alpha_m + (\alpha_c - \alpha_m)\left(\frac{2z+h}{2h}\right)^k\right) T dz
\end{aligned}
\tag{15}
$$

A FG circular and annular is considered to be embedded in a Visco-Pasternak elastic medium. The geometric properties of the nanoplate are denoted by outer radius *a,* inner radius *b,* thickness *h*. For convenience and generality we introduce the following non-dimensional parameters:

$$
\begin{aligned}
&W = \frac{w}{a},\ \xi = \frac{r}{a},\ \zeta = \frac{r}{b},\ \beta = \frac{b}{a},\ \psi_i = \frac{l_i}{h},\ \beta_0 = \frac{B' l_0^2}{C'},\ \beta_1 = \frac{B' l_1^2}{C'},\ \beta_2 = \frac{B' l_2^2}{C'},\ \overline{\mathrm{K}}_W = \frac{K_W a^4}{C'}\\
&\overline{\mathrm{C}} = \frac{C_d a^2}{C'}\sqrt{\frac{C'}{D'}},\ \overline{\mathrm{K}}_G = \frac{K_G a^2}{C'},\ \overline{\mathrm{P}} = \frac{N_0 a^2}{C'},\ \mathrm{P}^* = \frac{N_0 a^2}{C'},\ \hat{\lambda} = \frac{A'}{C'},\ \Omega^2 = D' \frac{\omega^2 a^4}{C'}, x^2 = \frac{E'}{D'}, \tau = \frac{t}{a^2}\sqrt{\frac{C'}{D'}}
\end{aligned}
\tag{16}
$$

Using the above expressions, a non-dimensional differential equation for vibration of FG circular and annular nanoplate in the thermal environment can be obtained

$$
\begin{aligned}
&\left\{2\psi_0^2 \hat{\lambda} + \frac{4\psi_1^2}{5}\hat{\lambda}\right\}\frac{\partial^6 W}{\partial \xi^6} + \left\{\frac{6\psi_0^2}{\xi}\hat{\lambda} + \frac{12\psi_1^2}{5\xi}\hat{\lambda}\right\}\frac{\partial^5 w}{\partial \xi^5} - \left\{1 + \beta_2 + 2\beta_0 + \frac{2\psi_1^2}{15\xi^2}\hat{\lambda} + \frac{8}{15}\beta_1\right\}\frac{\partial^4 w}{\partial \xi^4}\\
&- \left\{\frac{2}{\xi} + \frac{2}{\xi}\beta_2 + \frac{4}{\xi}\beta_0 + \frac{12\psi_0^2}{\xi^3}\hat{\lambda} - \frac{16}{15\xi}\beta_1 + \frac{4\psi_1^2}{15\xi^3}\hat{\lambda}\right\}\frac{\partial^3 w}{\partial \xi^3}\\
&+ \left\{\frac{1}{\xi^2} + \frac{1}{\xi^2}\beta_2 - \frac{18\psi_0^2}{\xi^4}\hat{\lambda} + \frac{2}{\xi^2}\beta_0 + \frac{8}{15\xi^2}\beta_1 + \overline{\mathrm{P}} + \mathrm{P}^* + \overline{\mathrm{K}}_G\right\}\frac{\partial^2 w}{\partial \xi^2}\\
&+ \left\{-\frac{1}{\xi^3} - \frac{1}{\xi^3}\beta_2 + \frac{18\psi_0^2}{\psi^5}\hat{\lambda} - \frac{2}{\xi^3}\beta_0 - \frac{8}{15\xi^3}\beta_1 + \frac{12\psi_1^2}{15\xi^4}\hat{\lambda} + \frac{\overline{\mathrm{P}}}{\xi} + \frac{\mathrm{P}^*}{\xi} + \frac{\overline{\mathrm{K}}_G}{\xi}\right\}\frac{\partial w}{\partial \xi}\\
&- \overline{\mathrm{K}}_W W - \overline{C}\frac{\partial W}{\partial \tau} - \frac{I_1 a^4}{C'}\frac{\partial^2 W}{\partial \tau^2} + \frac{I_2 a^2}{C'}\frac{\partial^4 W}{\partial \tau^2 \partial \xi^2} = 0
\end{aligned}
\tag{17}
$$

In order to obtain the governing equation of the classical FG circular and annular plate, one can insert the size dependent parameters set equal to zero ($l_0 = l_1 = l_2 = 0$). Also, with the assumption $l_0 = l_1 = 0$ in the Eq. (17) the governing equation of the circular and annular plate will be obtained by the MCST. The Eq. (17) is rewritten as the following form:

$$
[M]\{\ddot{d}\} + [C]\{\dot{d}\} + [K]\{d\} = 0 \tag{18}
$$

In the above equation, the matrices $[M],[C]$ and $[K]$ are the mass, damper and stiffness matrix, respectively. By defining the new freedom vector and general solution of the Eq. (17) as the following form:

© 2016 IAU, Arak Branch

$$\{Q\}=\begin{Bmatrix} d \\ \dot{d} \end{Bmatrix}, \qquad \mathrm{W(r,\tau)}=\{Q\}e^{\eta\tau} \tag{19}$$

By using the Eq. (19), we can rewrite the Eq. (18) as:

$$\left(\eta[A]+[B]\right)\{Q\}=0, \quad [A]=\begin{bmatrix} [0] & [M] \\ [I] & [0] \end{bmatrix}, \quad [B]=\begin{bmatrix} [K] & [C] \\ [0] & -[I] \end{bmatrix} \tag{20}$$

In the above equation, the η is a complex number and the vibration frequency of the FG circular and annular nanoplate is the imaginary part of the η .The elements of the stiffness, mass and damper matrix are given in the Eq. (21), respectively.

$$\begin{aligned}
[K] &= \left\{2\psi_0^2\lambda+\frac{4\psi_1^2}{5}\lambda\right\}\frac{d^6}{d\xi^6}(\bullet)+\left\{\frac{6\psi_0^2}{\xi}\lambda+\frac{12\psi_1^2}{5\xi}\lambda\right\}\frac{d^5}{d\xi^5}(\bullet) \\
&-\left\{1+\beta_2+2\beta_0+\frac{2\psi_1^2}{15\xi^2}\lambda+\frac{8}{15}\beta_1\right\}\frac{d^4}{d\xi^4}(\bullet)-\overline{\mathrm{K}}_W(\bullet) \\
&-\left\{\frac{2}{\xi}+\frac{2}{\xi}\beta_2+\frac{4}{\xi}\beta_0+\frac{12\psi_0^2}{\xi^3}\lambda-\frac{16}{15\xi}\beta_1+\frac{4\psi_1^2}{15\xi^3}\lambda\right\}\frac{d^3}{d\xi^3}(\bullet) \\
&+\left\{\frac{1}{\xi^2}+\frac{1}{\xi^2}\beta_2-\frac{18\psi_0^2}{\xi^4}\lambda+\frac{2}{\xi^2}\beta_0+\frac{8}{15\xi^2}\beta_1+\overline{\mathrm{P}}+\mathrm{P}^*+\overline{\mathrm{K}}_G\right\}\frac{d^2}{d\xi^2}(\bullet) \\
&+\left\{-\frac{1}{\xi^3}-\frac{1}{\xi^3}\beta_2+\frac{18\psi_0^2}{\psi^5}\lambda-\frac{2}{\xi^3}\beta_0-\frac{8}{15\xi^3}\beta_1+\frac{12\psi_1^2}{15\xi^4}\lambda+\frac{\overline{\mathrm{P}}}{\xi}+\frac{\mathrm{P}^*}{\xi}+\frac{\overline{\mathrm{K}}_G}{\xi}\right\}\frac{d}{d\xi}(\bullet) \\
[C] &= -\overline{C}(\bullet) \\
[M] &= +\frac{I_2a^2}{C'}\frac{d^2}{d\xi^2}(\bullet)-\frac{I_1a^4}{C'}(\bullet)
\end{aligned} \tag{21}$$

3 SOLUTION PROCEDURE

3.1 Solution FG circular nanoplate by Galerkin method

Eq. (17) is a sixth-order ordinary differential equation in ξ . If it is not impossible to solve the governing equation analytically, it is very difficult to obtain such a solution. Hence, approximate numerical method should be used. In the present study, Galerkin method is employed for the solution of the governing equation. The Galerkin method is a powerful and efficient numerical technique to solve the differential equations. Since this numerical method provides simple formulation and low computational cost, it has been widely used for the analysis of mechanical behavior of the structural elements at large and small scales, such as static, dynamic and stability problems [49, 50]. Furthermore, Galerkin's method is more general than the Rayleigh–Ritz method because no quadratic functional or virtual work principle is necessary.

On the hands and to the best of authors' knowledge, no satisfactory variational principle has been reported for the axisymmetric vibration of FG circular nanoplates yet. Using the general procedure of the method yields the following:

$$\iint_{\Omega}\bar{Q}\left(\sum_{j=1}^{n}A_jf_j(\xi)\right)f_k(\xi)d\Omega \tag{22}$$

where $f_j(\xi)$ $(j=1,2,...,n)$ are the basic functions which must satisfy all boundary conditions but not necessarily satisfy the governing equation. $A_j(j=1,2,...,n)$ are unknown coefficients to be determined. The integration extends

© 2016 IAU, Arak Branch

over the entire domain of the plate Ω. The symbol $\bar{Q}$ indicates a differential operator and is the right-hand side of Eq. (22).

Here, the boundary conditions (BC) for the FG circular of constant thickness along the edge $\xi = 1$ are assumed to be clamped. The boundary conditions are mathematically written as $W = dW/d\xi = 0$ at $\xi = 1$. In the Galerkin method, the lateral deflection can be described by a linear combination of the basic functions for the numerical solutions of the problem under investigation. The basic functions must satisfy all the above-mentioned boundary conditions. The chosen basic function for $W(\xi)$ are

$$f_j(\xi) = \xi^{2(j-1)}\left(1-\xi^2\right)^2 \tag{23}$$

Using Eq. (22), Eq. (23) and (20), one can obtain the following system of linear algebraic equations

$$\begin{aligned}
&\left(\left[B^*\right]+\eta\left[A^*\right]\right)\{Q\}=0\\
&A^*_{k,j}=\int_0^1 \xi^{2k-1}\left(1-\xi^2\right)^2\begin{bmatrix}[0] & [M]\left(\xi^{2(j-1)}\left(1-\xi^2\right)^2\right)\\ [I]\left(\xi^{2(j-1)}\left(1-\xi^2\right)^2\right) & [0]\end{bmatrix}d\xi\\
&B^*_{k,j}=\int_0^1 \xi^{2k-1}\left(1-\xi^2\right)^2\begin{bmatrix}[K]\left(\xi^{2(j-1)}\left(1-\xi^2\right)^2\right) & [C]\left(\xi^{2(j-1)}\left(1-\xi^2\right)^2\right)\\ [0] & -[I]\left(\xi^{2(j-1)}\left(1-\xi^2\right)^2\right)\end{bmatrix}d\xi
\end{aligned} \tag{24}$$

Here *M,C* and *I* are differential operators and are given in the Eq. (21).

The Galerkin method transforms the vibration problem into a standard eigenvalue problem. The vibration frequency parameter η is the eigenvalue of Eq. (24) that can be found by using standard eigenvalue extraction techniques.

3.2 DQM solution

In this section, for the solution of Eq. (18) the differential quadrature method (DQM) [51] is employed. DQM is an efficient numerical method for the solution of partial and ordinary differential equations. DQ technique can be used to deal with complicated problems reasonably well because its implementation is very simple. In comparison with other approximate numerical methods such as the finite elements method (FEM), the finite difference method, the boundary element method and the meshless methods, in this approach, the problem formulation becomes simpler and also low computational efforts are required to obtain acceptable solutions. In addition, since the strong form of the governing equations and the related boundary conditions are discretized in this method, they are free of the shear locking phenomenon that occurs in the FEM. In the review paper of Bert and Malik [52], some other advantages and disadvantages of the DQ technique are also reported. In recent years, many researchers used DQ approach for the global behavior analysis of the nanostructural elements, such as elastic buckling of single-layered graphene sheets [53, 54].

The DQM is based on a simple mathematical concept that a partial derivative of a function with respect to a space variable at a discrete mesh point (grid point) in domain can be approximated by taking a weighted linear sum of the functional values at all grid points in the whole domain. According to DQ method, the partial derivatives of a function $f(r)$ as an example, at the point (r_i) are expressed as: [51,52]

$$\frac{d^s f(r)}{dr^s}\Big|_{r=r_i} = \sum_{j=1}^{n} C_{ij}^s f(r_j),\ \ i = 1,2,...,n \tag{25}$$

where n is the number of grid points in the r direction. C_{ij}^s represents the respective weighting coefficient related to the *S*th-order derivative. According to Shu and Richard rule [51], the weighting coefficients in *r* direction are determined as, If $S = 1$ namely, for the first order derivative,

© 2016 IAU, Arak Branch

$$C_{ij}^{1}=\frac{M^{(1)}(r_i)}{(r_i-r_j)M^{(1)}(r_j)} \quad \text{for } i\neq j \text{ and } i,j=1,2,...,n \tag{26}$$

and

$$C_{ii}^{1}=-\sum_{j=1(j\neq i)}^{n} C_{ij}^{1} \quad \text{for } i=j \text{ and } i=1,2,...,n \tag{27}$$

where $M^{(1)}(r)$ is the first order derivative of $M(r)$ and they can be expressed as:

$$M(r)=\prod_{j=1}^{n}(r-r_j),\ \ M^{(1)}(r_k)=\prod_{j=1(j\neq k)}^{n}(r_k-r_j) \tag{28}$$

If $s>1$, namely, for the second derivatives, the weighting coefficients are obtained by using the following simple recursion relationship

$$C_{ij}^{2}=\sum_{k=1}^{n}C_{ik}^{1}C_{kj}^{1},\ \ C_{ij}^{3}=\sum_{k=1}^{n}C_{ik}^{1}C_{kj}^{2},\ \ C_{ij}^{4}=\sum_{k=1}^{n}C_{ik}^{1}C_{kj}^{3} \quad \text{for } i,j=1,2,...n \tag{29}$$

One key point in the successful application of the differential quadrature method is how to select the grid points. It has been shown that the grid point distribution which is based on well accepted Gauss-Chebyshev–Lobatto points [52], gives sufficiently accurate results. According to this grid point's distribution, the grid point distribution in the ζ direction for annular and circular FG nanoplate are given as the following form [51]

$$\zeta_i=\beta+\frac{(1-\beta)}{2}\left(1-\cos\left(\frac{(i-1)\pi}{(N-1)}\right)\right),\ \ i=1,2,...,N \qquad \zeta_i=\frac{1}{2}\left[1-\cos\left(\frac{i-1}{n-1}\pi\right)\right],\ \ i=1,2,...,n \tag{30}$$

The non-dimensional computational domain of the nanoplate is $0\le\zeta\le1$. Using the DQ method, Eq. (21) can be discretized as:

$$\begin{aligned}
[K]=&\left\{2\psi_0^2\lambda+\frac{4\psi_1^2}{5}\lambda\right\}\sum_{j=1}^{n}C_{ij}^{6}W_j+\left\{\frac{6\psi_0^2}{\xi}\lambda+\frac{12\psi_1^2}{5\xi}\lambda\right\}\sum_{j=1}^{n}C_{ij}^{5}W_j\\
&-\left\{1+\beta_2+2\beta_0+\frac{2\psi_1^2}{15\xi^2}\lambda+\frac{8}{15}\beta_1\right\}\sum_{j=1}^{n}C_{ij}^{4}W_j-\overline{\mathrm{K}}_W W_i\\
&-\left\{\frac{2}{\xi}+\frac{2}{\xi}\beta_2+\frac{4}{\xi}\beta_0+\frac{12\psi_0^2}{\xi^3}\lambda-\frac{16}{15\xi}\beta_1+\frac{4\psi_1^2}{15\xi^3}\lambda\right\}\sum_{j=1}^{n}C_{ij}^{3}W_j\\
&+\left\{\frac{1}{\xi^2}+\frac{1}{\xi^2}\beta_2-\frac{18\psi_0^2}{\xi^4}\lambda+\frac{2}{\xi^2}\beta_0+\frac{8}{15\xi^2}\beta_1+\overline{\mathrm{P}}+\mathrm{P}^*+\overline{\mathrm{K}}_G\right\}\sum_{j=1}^{n}C_{ij}^{2}W_j\\
&+\left\{-\frac{1}{\xi^3}-\frac{1}{\xi^3}\beta_2+\frac{18\psi_0^2}{\psi^5}\lambda-\frac{2}{\xi^3}\beta_0-\frac{8}{15\xi^3}\beta_1+\frac{12\psi_1^2}{15\xi^4}\lambda+\frac{\overline{\mathrm{P}}}{\xi}+\frac{\mathrm{P}^*}{\xi}+\frac{\overline{\mathrm{K}}_G}{\xi}\right\}\sum_{j=1}^{n}C_{ij}^{1}W_j\\
[C]=&-\overline{C}W_i\\
[M]=&+\frac{I_2a^2}{C'}\sum_{j=1}^{n}C_{ij}^{2}W_j-\frac{I_1a^4}{C'}W_i
\end{aligned} \tag{31}$$

where W_j is the functional value at the grid point $\zeta=\zeta_j$. It should be noted that Eq. (31) is solved for inner grid points. The inner grid points are calculated by considering the boundary conditions in the Eq. (13). The boundary conditions are incorporated in the analysis by direct substitution of them into the discrete governing equation [51].

© 2016 IAU, Arak Branch

The derivatives in the boundary conditions are also discretized by the DQ procedure. After implementation of the boundary conditions, the Eq. (31) can be written in the following form:

$$
\begin{aligned}
[K] &= \left\{2\psi_0^2\lambda + \frac{4\psi_1^2}{5}\lambda\right\}\sum_{j=2}^{n-1}\hat{C}_{ij}^6 W_j + \left\{\frac{6\psi_0^2}{\xi}\lambda + \frac{12\psi_1^2}{5\xi}\lambda\right\}\sum_{j=2}^{n-1}\hat{C}_{ij}^5 W_j \\
&-\left\{1+\beta_2+2\beta_0+\frac{2\psi_1^2}{15\xi^2}\lambda+\frac{8}{15}\beta_1\right\}\sum_{j=2}^{n-1}\hat{C}_{ij}^4 W_j - \overline{\mathrm{K}}_W W_i \\
&-\left\{\frac{2}{\xi}+\frac{2}{\xi}\beta_2+\frac{4}{\xi}\beta_0+\frac{12\psi_0^2}{\xi^3}\lambda-\frac{16}{15\xi}\beta_1+\frac{4\psi_1^2}{15\xi^3}\lambda\right\}\sum_{j=2}^{n-1}\hat{C}_{ij}^3 W_j \\
&+\left\{\frac{1}{\xi^2}+\frac{1}{\xi^2}\beta_2-\frac{18\psi_0^2}{\xi^4}\lambda+\frac{2}{\xi^2}\beta_0+\frac{8}{15\xi^2}\beta_1+\overline{\mathrm{P}}+\mathrm{P}^*+\overline{\mathrm{K}}_G\right\}\sum_{j=2}^{n-1}\hat{C}_{ij}^2 W_j \\
&+\left\{-\frac{1}{\xi^3}-\frac{1}{\xi^3}\beta_2+\frac{18\psi_0^2}{\psi^5}\lambda-\frac{2}{\xi^3}\beta_0-\frac{8}{15\xi^3}\beta_1+\frac{12\psi_1^2}{15\xi^4}\lambda+\frac{\overline{\mathrm{P}}}{\xi}+\frac{\mathrm{P}^*}{\xi}+\frac{\overline{\mathrm{K}}_G}{\xi}\right\}\sum_{j=2}^{n-1}\hat{C}_{ij}^1 W_j \\
[C] &= -\bar{C}W_i \\
[M] &= +\frac{I_2 a^2}{C'}\sum_{j=2}^{n-1}\hat{C}_{ij}^2 W_j - \frac{I_1 a^4}{C'}W_i
\end{aligned}
\tag{32}
$$

where

$$
\bar{\Sigma}_i^s = \sum_{j=2}^{n-1}\hat{C}_{ij}^s W_j,\quad \hat{C}_{ij}^s = C_{ij}^s - C_{i1}^s C_{nj}^1 / C_{n1}^1 \quad \text{for } i=1,2,...,n \text{ and } s=1,2,...,6 \tag{33}
$$

After employing the aforementioned solution procedure, one obtains the following system of linear algebraic equations

$$
\left(\eta[A]+[B]\right)\{Q\} = 0 \tag{34}
$$

where $[A]$ and $[B]$ are $(n-2)\times(n-2)$ square matrices. The elements of these matrices are easily obtained from the Eq. (20). Again, it is observed that non-dimensional buckling load η can be determined from the eigenvalues of a system of algebraic equations and this parameter is a complex number that the imaginary part is the vibration frequency of the FG circular and annular nanoplate.

4 NUMERICAL RESULTS AND COMPARISONS

The combination of materials consists of aluminum and ceramic SiC. The Young's modulus, coefficient of thermal expansion, the density and Poison ratio for aluminum are $E_m = 70$ GPa, $\alpha_m = 23\times10^{-6}$, $\rho_m = 2702\ kg/m^3$ and $\upsilon_m = 0.3$, respectively. These parameters for the ceramic are $E_c = 427$ GPa, $\alpha_c = 7.4\times10^{-6}$, $\rho_c = 3100\ kg/m^3$ and $\upsilon_c = 0.17$, respectively. These material parameters are reported by Ke et al. [55]. The method of this paper can deal with all kinds of combinations of clamped and simply supported boundary conditions. Natural frequency parameters are listed in tables. The existing local plate model solutions are used for verification of the accuracy of circular and annular results. Following four boundary conditions have been investigated in the vibration analysis of the annular graphene sheets.

SS: Annular graphene sheet with simply supported outer and inner radius.
CS: Annular graphene sheet with clamped outer and simply supported inner radius.
SC: Annular graphene sheet with simply supported outer and clamped inner radius.
CC: Annular graphene sheet with clamped outer and inner radius.

© 2016 IAU, Arak Branch

4.1 Validation of present computed results

The present size dependent model can easily reduce to the classical circular and annular plate model with the size effect being neglected in the constitutive relations. To confirm the reliability of the present formulation and results, comparison studies are conducted for the natural frequencies of the circular plate without considering size dependent parameters. Table 1. tabulates the comparison of the vibration frequency parameters for circular plates. It is seen that the present results for all the two boundary conditions are in excellent agreement with the classical results.

Table 1
Comparison of the present results with natural frequency parameters of classical plate theory $\Omega = \sqrt{\rho h / C'}\omega a^2$.

	References					
Boundary condition	Leissa and Narita [56]	Kim and Dickinson [57]	Li and Li [58]	Zhou et al. [59]	Present	
simply supported boundary condition	13.898	13.898	13.898	13.898	13.8981	
clamped boundary condition	Carrington [60]	Kim and Dickinson [57]	Leissa [61]	Zhou et al. [59]	Present (DQM)	Present (Galerkin)
	21.260	21.260	21.26	21.260	21.2604	21.2602

Table 2. presents the comparison of the vibration frequency parameters for the annular plates. The annular plate solutions in Table 2. were found to be in good agreement with those non-dimensional natural frequency values obtained by previous researchers [62, 59] who have used other techniques. All the results are presented for the four boundary conditions.

Table 2
Comparison of the present results with classical plate theory for the lowest six natural frequency parameters $\left(\Omega = \omega a^2\sqrt{\rho h / C'},\ \beta = b/a = 0.4\right)$.

	References		
Boundary condition	Chakraverty et al. [62]	Zhou et al. [59]	Present
CC	63.04	62.996	62.996
SS	30.09	30.079	30.124
SC	42.63	42.548	42.5858
CS	46.74	46.735	46.5558

For further validation, the present results are compared with the first three natural frequencies of the FG annular microplate in Table 3. Since there are no published results available for annular nanoplates in open literature, the results of annular microplate are used for comparison. To obtain these results, the modified couple stress theory is utilized. From this table, one can see that the present results are in good agreement with the reported results in the literature. To obtain the natural frequencies of the FG annular plate, the boundary condition of annular microplate are assumed SS and CC. The other material properties of the annular microplate are reported by Ke et al. [55].

Table 3
Comparison of the present results with MCST for the natural frequency parameters of annular FG microplate $(\beta = b/a = 0.5,\ \psi = 0.5,\ \mathrm{k} = 2)$.

Boundary condition	References					
	First Mode		Second Mode		Third Mode	
	Ke et al. [55]	Present	Ke et al. [55]	Present	Ke et al. [55]	Present
CC	5.5364	5.53639	8.3238	8.32377	12.5300	12.5301
SS	3.2665	3.2662	7.9057	7.90568	10.1756	10.17564

A computer code is developed in MATLAB based on Eq. (20). As DQ results are sensitive to lower grid points, a convergence test is performed to determine the minimum number of grid points required to obtain stable and accurate results for Eq. (20). The analysis is carried out by radius of nanoplate 10 *nm*, the size dependent parameter 0.5 *nm*, the shear, Winkler and damping coefficients are assumed 10, 100 and 10, respectively. According to the Fig.

© 2016 IAU, Arak Branch

2, present solution is convergent. From the figure it is clearly seen that eleventh number of grid points ($N_\xi = 11$) are sufficient to obtain the accurate solutions for the present analysis.

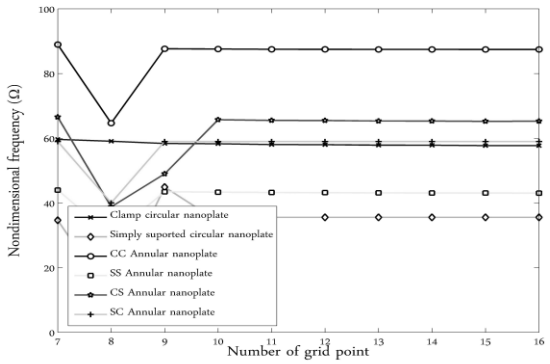

Fig.2
Convergence study and minimum number of grid points (N_ζ) required to obtain accurate results.

4.2 The results of present study

Variation of vibration frequency versus compressive in-plane pre-load is shown for FG circular nanoplate in the Fig. 3. The non-dimensional parameter of elastic medium such as shear modulus parameter $\overline{K}_G$, Winkler modulus parameter $\overline{K}_W$ and damping modulus of damper $\overline{C}$ for the surrounding polymer matrix is gotten 10, 100 and 10 respectively. The curves show that the vibration frequency is sensitive to the modulus of the surrounding elastic medium. It is also clearly shown that the vibration frequency decreases by increasing the in-plane pre-load. Further, it is illustrated that the damping modulus decreases the vibration frequency; thus, the greatest and the smallest vibration frequency are belong to the FG nanoplate based on the Pasternak medium and Visco-Winkler medium, respectively.

To determine the effect of the aspect ratio on the vibration frequency of the FG nanoplate, the vibration frequencies of the FG annular nanoplate against the aspect ratio are plotted in the Fig. 4 for four different boundary conditions. To obtain the results, the vibration frequencies are presented by considering the power index parameter 10 and the inner radius 40 *nm*. Also, the size dependent parameter is assumed 0.5*h* in the MSGT. From this figure, it is clearly shown that the non-dimensional frequency increases with the increase of the aspect ratio. Also, the results show that the non-dimensional frequency increases monotonically by increasing the rigidity of the boundary conditions. In Fig. 4, the gap between the curves increases with increasing the aspect ratio.

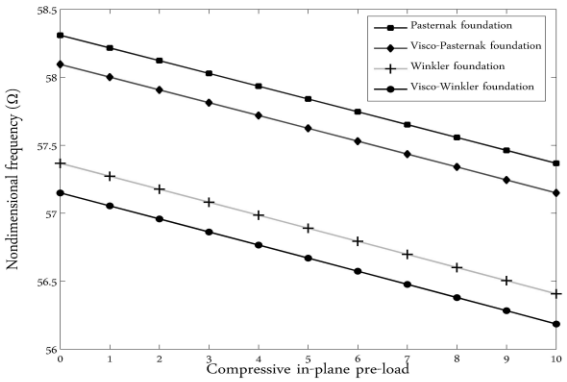

Fig.3
Variation of vibration frequency with the compressive pre-load for various kind of elastic medium.

© 2016 IAU, Arak Branch

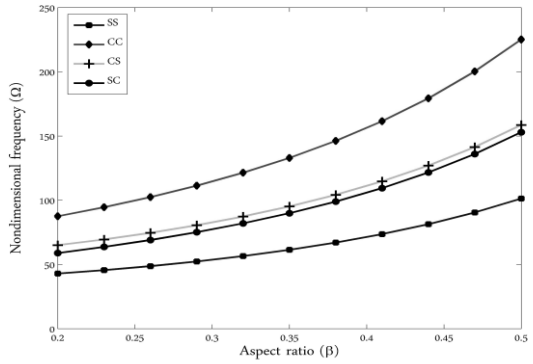

Fig.4
Variation of vibration frequency with the aspect ratio for various boundary conditions.

The first vibration frequencies of the circular FG nanoplate are plotted in the Fig. 5. In these figures, the dependency of the vibration frequency versus the radius of the circular FG nanoplate is shown for different temperature changes. To obtain these results, it is assumed that the FG nanoplate embedded on a visco-Pasternak foundation and the shear elastic, the Winkler elastic and the external damping coefficient are assumed 10, 100 and 100, respectively. Also, the power index of FG material and the size dependent length of the circular nanoplate are considered 10, and $0.5h$, respectively. The vibration frequencies are obtained by considering the modified strain gradient theory. From this figure, it is clear that the vibration frequency of the circular nanoplate is strongly depend on the radius of the circular nanoplate and this dependency is more for the larger temperature change. Also, the effect of the temperature change decreases with decreasing the radius of the nanoplate. Furthermore, this figure shows that the temperature change has a decreasing effect on the vibration frequency of the circular nanoplate. According to this figure, one can easily find that the natural frequency is strongly depended to the radius of the nanoplate and this parameter has a decreasing effect on the natural frequency of the FG nanoplate. Moreover, this figure indicates that there is critically temperature and radius for the FG nanoplate because the vibration frequency becomes zero in a specific radius and temperature change; thus, this specific radius and temperature change is called the critically parameters.

Influence of the size dependent on the frequencies of nanoplate under the temperature change by considering the modified couple stress and the modified strain gradient theory is studied. Fig. 6 shows the variation in vibration frequency with size dependent parameter under various power index parameters. The nanoplate is assumed to be subjected to a temperature change of $\Delta T = 50$. It can be observed that as the size dependent parameter increases, the non-dimensional frequency increases for all values of the power index parameter. The results of figure indicate that, by increasing the values of size dependent parameter, the difference between the MCST and the MSGT is increased for all values of power index parameters. It is also observed that as the power index parameter increases the vibration frequency decreases. Furthermore, as can be seen from Fig. 6, the non-dimensional frequency is sensitive to the size dependent parameter for small values of power index parameter. In the other words, it is seen that the non-dimensional frequency for FG nanoplates with higher size dependent parameter are strongly affected by the used elasticity theory (MSGT and MCST).

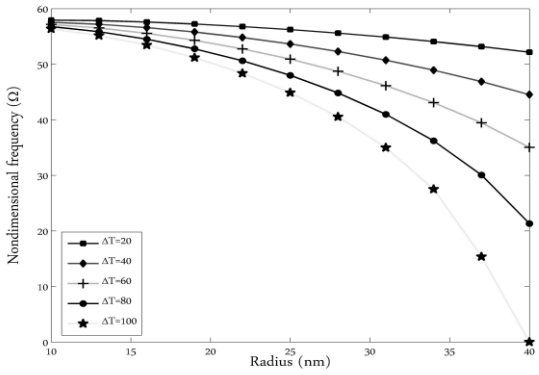

Fig.5
Variation of vibration frequency with the radius of circular FG nanoplate for various temperature changes.

© 2016 IAU, Arak Branch

To see the effect of temperature change in different power index parameter from the solution for non-dimensional frequency FG annular nanoplate with different length are shown in Fig. 7. The variation of non-dimensional natural frequency for FG annular nanoplate with CC and SS boundary condition is plotted in Fig. 7. The aspect ratio of nanoplate is considered 0.4. It is found that the non-dimensional frequency increases with increase of the rigidity of the boundary condition for all lengths. Similar vibration response as this trend is observed for other boundary conditions. The results are shown that the vibration frequency of the FG annular nanoplate by high power index parameter is lower than that the vibration frequency of the FG nanoplate by low power index parameter. It is also observed that the effect of the temperature change on the non-dimensional frequency is important for SS annular nanoplate with high power index parameter in comparison with the annular nanoplate with rigidity boundary condition and small power index parameter.

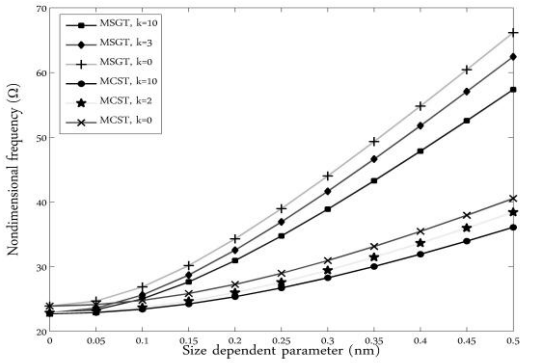

Fig.6
Variation of vibration frequency with the size dependent parameters of the FG nanoplate for various power index parameter and two different elasticity theories.

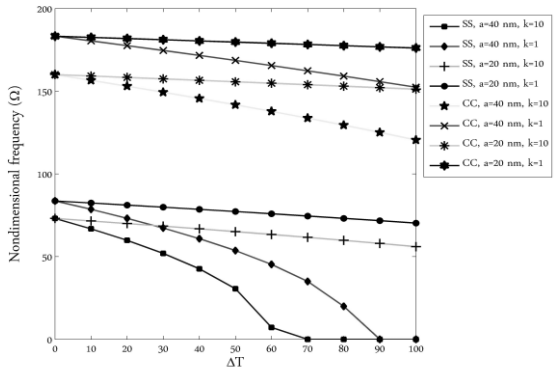

Fig.7
Variation of vibration frequency with the temperature change of the FG annular nanoplate for various power index parameter, radius and boundary conditions.

In order to show the dependency of the higher vibration frequency mode of the viscoelastic nanoplate on the foundation type and size dependent parameter, the size dependent difference percentage is introduced as follows:

$$\text{Size dependent difference p}\textit{ercentage} = \left| \frac{\text{Vibration } \textit{frequency}_{\psi \neq 0} - \text{Vibration } \textit{frequency}_{\psi = 0}}{\text{Vibration } \textit{frequency}_{\psi = 0}} \right| \times 100$$

To this end, the size dependent difference percentage versus size dependent parameter is plotted in the Fig. 8 for various kind of elastic foundation and three different vibration frequency modes. The aspect ratio of the circular annular nanoplate is assumed 0.4; also, the outer and inner boundary condition of the annular nanoplate are considered clamp. From this figure, it is clear that the vibration frequency of the nanoplate is strongly depend on the size dependent and the kind of the elastic foundation and this dependency is more for the higher mode vibration frequency. Also, the effect of the size dependent on the first vibration frequency mode is more than that the third vibration frequency mode. On the other hand, the effect of the elastic foundation on the vibration frequency is more important for the first vibration frequency mode in comparison with the third vibration frequency mode. Further, one can easily see that the effect of the size dependent on the vibration frequency mode for the nanoplate with the Winkler foundation is more important than the nanoplate with Visco-Pasternak foundation.

© 2016 IAU, Arak Branch

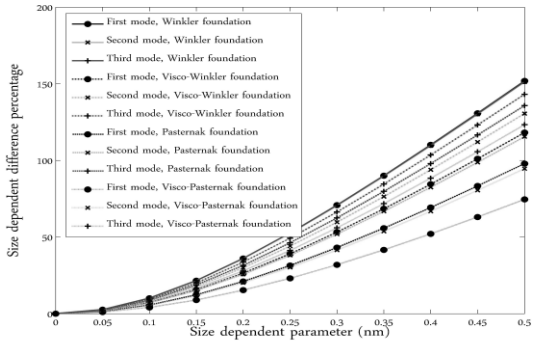

Fig.8
Variation of size dependent difference percentage with the size dependent parameter for various kind of elastic foundation and three different frequency mode.

5 CONCLUSIONS

This study illustrates the significance of size dependent effects on the vibration behavior of FG circular and annular nanoplate in the thermal environment. Two different size dependent continuum theories (MSGT and MCST) are utilized to obtain the vibration frequencies of the FG annular and circular nanoplate. To calculate the natural frequencies, the differential quadrature method and the Galerkin method are used. The results are presented for clamp and simply supported FG circular nanoplate. The vibration frequencies of the annular nanoplate with four different boundary conditions are also obtained. From the results following conclusions are noticeable:

- The vibration frequency of the FG circular and annular nanoplate is strongly depended on the radius of the circular nanoplate and this dependency is more for the larger temperature change.
- The influence of temperature change reduces, by decreasing of radius.
- The non-dimensional natural frequency decreases at high temperature case with increasing the temperature change.
- The effect of temperature change on the non-dimensional frequency vibration becomes the opposite at low temperature case in compression with the high temperature case.
- The power index effect for the MSGT is much more than that for the MCST.
- The power index effect has a decreasing effect on the vibration frequency of the FG circular and annular effect.
- The size dependent parameter has an increasing effect and this parameter play an important role in the case of FG circular and annular nanoplate with smaller power index parameter.
- The differences between the vibration responses of the FG nanoplate increase by increasing the size dependent parameter.
- The effect of temperature on the frequency vibration increases with increasing the radius of annular nanoplate.
- The effect of temperature change is significant to predict the mechanical behavior of FG circular and annular nanoplate with high power index parameter and cannot be ignored.
- In the first mode, the effect of the elastic foundation on the vibration frequency is more important in comparison with the third vibration frequency mode.
- The effect of the size dependent on the first vibration frequency mode is more than that the third vibration frequency mode.

REFERENCES

[1] Sallese J.M., Grabinski W., Meyer V., Bassin C., Fazan P., 2001, Electrical modeling of a pressure sensor MOSFET, *Sensors* and *Actuators A*: *Physical* **94**: 53-58.

[2] Nabian A., Rezazadeh G., Haddad-derafshi M., Tahmasebi A., 2008, Mechanical behavior of a circular microplate subjected to uniform hydrostatic and non-uniform electrostatic pressure, *Microsystem Technologies* **14**: 235-240.

[3] Bao M., Wang W., 1996, Future of microelectromechanical systems (MEMS), *Sensors* and *Actuators A*: *Physical* **56**: 135-141.

© 2016 IAU, Arak Branch

[4] Younis M.I., Abdel-Rahman E.M., Nayfeh A., 2003, A reduced-order model for electrically actuated microbeambased MEMS, *Journal of Microelectromechanical Systems* **12**: 672-680.
[5] Batra R.C., Porfiri M., Spinello D, 2006, Electromechanical model of electrically actuated narrow microbeams, *Journal of Microelectromechanical Systems* **15**: 1175-1189.
[6] Nayfeh A.H., Younis M.I., Abdel-Rahman E.M., 2007, Dynamic pull-in phenomenon in MEMS resonators, *Nonlinear Dynamics* **48**: 153-163.
[7] Nayfeh A.H., Younis M.I., 2004, Modeling and simulations of thermoelastic damping in microplates, *Journal of Micromechanics and Microengineering* **14**: 1711-1717.
[8] Zhao X.P., Abdel-Rahman E.M., Nayfeh A.H., 2004, A reduced-order model for electrically actuated microplates, *Journal of Micromechanics and Microengineering* **14**: 900-906.
[9] Machauf A., Nemirovsky Y., Dinnar U., 2005, A membrane micropump electrostatically actuated across the working fluid, *Journal of Micromechanics and Microengineering* **15**: 2309-2316.
[10] Wong E.W., Sheehan P.E., Lieber C.M., 1997, Nanobeam mechanics: elasticity, strength and toughness of nanorods and nanotubes, *Science* **277**: 1971-1975.
[11] Zhou S.J., Li Z.Q., 2001, Metabolic response of Platynota stultana pupae during and after extended exposure to elevated CO2 and reduced O2 atmospheres, *Shandong University Technology* **31**: 401-409.
[12] Mohammadi V., Ansari R., Faghih Shojaei M., Gholami R., Sahmani S., 2013, Size-dependent dynamic pull-in instability of hydrostatically and electrostatically actuated circular microplates, *Nonlinear Dynamics* **73**: 1515-1526.
[13] Yang F., Chong A.C.M., Lam D.C.C., Tong P., 2002, Couple stress based strain gradient theory for elasticity, *International Journal of Solids and Structures* **39**: 2731-2743.
[14] Eringen A.C., 1983, On differential equations of nonlocal elasticity and solutions of screw dislocation and surface waves, *Journal Applied Physics* **54**: 4703-4711.
[15] Asemi H.R., Asemi S.R., Farajpour A., Mohammadi M., 2015, Nanoscale mass detection based on vibrating piezoelectric ultrathin films under thermo-electro-mechanical loads, *Physica E* **68**: 112-122.
[16] Danesh M., Farajpour A., Mohammadi M., 2012, Axial vibration analysis of a tapered nanorod based on nonlocal elasticity theory and differential quadrature method, *Mechanics Research Communications* **39**: 23-27.
[17] Aydogdu M., 2009, Axial vibration of the nanorods with the nonlocal continuum rod model, *Physica E* **41**: 861-864.
[18] Mohammadi M., Farajpour A., Goodarzi M., Heydarshenas R., 2013, Levy type solution for nonlocal thermo-mechanical vibration of orthotropic mono-layer graphene sheet embedded in an elastic medium, *Journal of Solid Mechanics* **5**(2): 116-132.
[19] Mohammadi M., Farajpour A., Goodarzi M., Dinari F., 2014, Thermo-mechanical vibration analysis of annular and circular graphene sheet embedded in an elastic medium, *Latin American Journal of Solids and Structures* **11** (4): 659-682.
[20] Duan W. H., Wang C. M., 2007, Exact solutions for axisymmetric bending of micro/nanoscale circular plates based on nonlocal plate theory, *Nanotechnology* **18**: 385704.
[21] Mohammadi M., Moradi A., Ghayour M., Farajpour A., 2014, Exact solution for thermo-mechanical vibration of orthotropic mono-layer graphene sheet embedded in an elastic medium, *Latin American Journal of Solids and Structures* **11**(3): 437-458.
[22] Asemi S.R., Farajpour A., Asemi H.R., Mohammadi M., 2014, Influence of initial stress on the vibration of double-piezoelectric-nanoplate systems with various boundary conditions using DQM, *Physica E* **63**: 169-179.
[23] Mohammadi M., Goodarzi M., Ghayour M. Farajpour A., 2013, Influence of in-plane pre-load on the vibration frequency of circular graphene sheet via nonlocal continuum theory, *Composites Part B* **51**: 121-129.
[24] Goodarzi M., Mohammadi M., Farajpour A., Khooran M., 2014, Investigation of the effect of pre-stressed on vibration frequency of rectangular nanoplate based on a visco pasternak foundation, *Journal of Solid Mechanics* **6**: 98-121.
[25] Farajpour A., Shahidi A. R., Mohammadi M., Mahzoon M., 2012, Buckling of orthotropic micro/nanoscale plates under linearly varying in-plane load via nonlocal continuum mechanics, *Composite Structures* **94**: 1605-1615.
[26] Mohammadi M., Farajpour A., Goodarzi M., Mohammadi H., 2013, Temperature effect on vibration analysis of annular graphene sheet embedded on visco-Pasternak foundation, *Journal of Solid Mechanics* **5**(3): 305-323.
[27] Wang C.M., Duan W.H., 2008, Free vibration of nanorings/arches based on nonlocal elasticity, *Journal of Applied Physics* **104**: 014303.
[28] Moosavi H., Mohammadi M., Farajpour A., Shahidi S. H., 2011, Vibration analysis of nanorings using nonlocal continuum mechanics and shear deformable ring theory, *Physica E* **44**: 135-140.
[29] Mohammadi M., Goodarzi M., Ghayour M., Alivand S., 2012, Small scale effect on the vibration of orthotropic plates embedded in an elastic medium and under biaxial in-plane pre-load via nonlocal elasticity theory, *Journal of Solid Mechanics* **4**(2) : 128-143.
[30] Wang B., Zhao J., Zhou S., 2010, A micro scale Timoshenko beam model based on strain gradient elasticity theory, *European Journal of Mechanics* A/*Solids* **29:** 591-599.
[31] Ansari R., Gholami R., Sahmani S., 2011, Free vibration of size-dependent functionally graded microbeams based on a strain gradient theory, *Composite Structures* **94**: 221-228.
[32] Ansari R., Gholami R., Sahmani S., 2012, Study of small scale effects on the nonlinear vibration response of functionally graded Timoshenko microbeams based on the strain gradient theory, *Journal of Computational and Nonlinear Dynamics* **7**: 031010 .

© 2016 IAU, Arak Branch

[33] Sahmani S., Ansari R., 2013, On the free vibration response of functionally graded higher-order shear deformable microplates based on the strain gradient elasticity theory, *Composite Structures* **95**: 430-442.
[34] Ghayesh M.H., Amabili M., Farokhi H., 2013, Nonlinear forced vibrations of a microbeam based on the strain gradient elasticity theory, *International Journal of Engineering Science* **63**: 52-60.
[35] Mohammadi M., Farajpour A., Moradi M., Ghayour M., 2013, Shear buckling of orthotropic rectangular graphene sheet embedded in an elastic medium in thermal environment, *Composites Part B: Engineering* **56**: 629-637.
[36] Civalek Ö., Akgöz B., 2013, Vibration analysis of micro-scaled sector shaped graphene surrounded by an elastic matrix, *Computational Materials Science* **77**: 295-303.
[37] Murmu T., Pradhan S.C., 2009, Vibration analysis of nano-single-layered graphene sheets embedded in elastic medium based on nonlocal elasticity theory, *Journal of Applied Physics* **105**: 064319.
[38] Pradhan S.C., Phadikar J.K., 2009, Small scale effect on vibration of embedded multi layered graphene sheets based on nonlocal continuum models, *Physics Letters A* **373**: 1062-1069.
[39] Wang Y. Z., Li F. M., Kishimoto K., 2011, Thermal effects on vibration properties of doublelayered nanoplates at small scales, *Composites Part B: Engineering* **42**: 1311-1317.
[40] Reddy C.D., Rajendran S., Liew K.M., 2006, Equilibrium configuration and continuum elastic properties of finite sized graphene, *Nanotechnology* **17**: 864-870.
[41] Aksencer T., Aydogdu M., 2011, Levy type solution method for vibration and buckling of nanoplates using nonlocal elasticity theory, *Physica E* **43**: 954-959.
[42] Malekzadeh P., Setoodeh A.R., Alibeygi Beni A., 2011, Small scale effect on the thermal buckling of orthotropic arbitrary straight-sided quadrilateral nanoplates embedded in an elastic medium, *Composite Structures* **93**: 2083-2089.
[43] Satish N., Narendar S., Gopalakrishnan S., 2012, Thermal vibration analysis of orthotropic nanoplates based on nonlocal continuum mechanics, *Physica E* **44**: 1950-1962.
[44] Prasanna Kumar T.J., Narendar S., Gopalakrishnan S., 2013, Thermal vibration analysis of monolayer graphene embedded in elastic medium based on nonlocal continuum mechanics, *Composite Structures* **100**: 332-342.
[45] Farajpour A., Mohammadi M., Shahidi A.R., Mahzoon M., 2011, Axisymmetric buckling of the circular graphene sheets with the nonlocal continuum plate model, *Physica E* **43**: 1820-1825.
[46] Mohammadi M., Ghayour M., Farajpour A., 2013, Free transverse vibration analysis of circular and annular graphene sheets with various boundary conditions using the nonlocal continuum plate model, *Composites Part B: Engineering* **45**: 32-42.
[47] Lam D.C.C., Yang F., Chong A.C.M., Wang J., Tong P., 2003, Experiments and theory in strain gradient elasticity, *Journal of the Mechanics and Physics of Solids* **51**: 1477-1508.
[48] Timoshenko S.P., Goodier J.N., 1970, *Theory of Elasticity*, McGraw-Hill, New York.
[49] Saadatpour M. M., Azhari M., 1998, The Galerkin method for static analysis of simply supported plates of general shape, *Computers and Structures* **69**: 1-9.
[50] Farajpour A., Danesh M., Mohammadi M., 2011, Buckling analysis of variable thickness nanoplates using nonlocal continuum mechanics, *Physica E* **44**: 719-727.
[51] Shu C., 2000, *Differential Quadrature and its Application in Engineering*, Berlin, Springer.
[52] Bert C.W., Malik M., 1996, Differential quadrature method in computational mechanics: a review, *Applied Mechanics Reviews* **49**: 1-27.
[53] Malekzadeh P., Setoodeh A. R., Alibeygi Beni A., 2011, Small scale effect on the thermal buckling of orthotropic arbitrary straight-sided quadrilateral nanoplates embedded in an elastic medium, *Composite Structures* **93**: 2083-2089.
[54] Wang Y. Z., Li F. M., Kishimoto K., 2011, Thermal effects on vibration properties of double-layered nanoplates at small scales, *Composites Part B: Engineering* **42**: 1311-1317.
[55] Ke L. L., Yang J., Kitipornchai S., Bradford M. A., 2012, Bending, buckling and vibration of size-dependent functionally graded annular microplates, *Composite Structures* **94**: 3250-3257.
[56] Leissa A.W., Narita Y., 1980, Natural frequencies of simply supported circular plates, *Journal of Sound and Vibration* **70**: 221-229.
[57] Kim C.S., Dickinson S.M., 1989, On the free, transverse vibration of annular and circular, thin, sectorial plates subject to certain complicating effects, *Journal of Sound and Vibration* **134**: 407-421.
[58] Qiang L.Y., Jian L., 2007, Free vibration analysis of circular and annular sectorial thin plates using curve strip Fourier P-element, *Journal of Sound and Vibration* **305**: 457-466.
[59] Zhou Z.H., Wong K.W., Xu X.S., Leung A.Y.T., 2011, Natural vibration of circular and annular thin plates by Hamiltonian approach, *Journal of Sound and Vibration* **330**: 1005-1017.
[60] Carrington H., 1925, The frequencies of vibration of flat circular plates fixed at the circumference, *Philosophical Magazine* **6**: 1261-1264.
[61] Leissa A.W., 1969, *Vibration of Plates*, Office of Technology Utilization, Washington.
[62] Chakraverty S., Bhat R.B., Stiharu I., 2001, Free vibration of annular elliptic plates using boundary characteristic orthogonal polynomials as shape functions in the Rayleigh–Ritz method, *Journal of Sound and Vibration* **241**: 524-539.

© 2016 IAU, Arak Branch